Enhancing a Distributed Electric Propulsion Configuration Aircraft Design with a Multidisciplinary Analysis and Optimization Approach

D. Granata[1], S. Mancini[2], A. Mateo-Gabin[3], A. Zanotti[1]

[1] Politecnico di Milano, Dipartimento di Scienze e Tecnologie Aerospaziali, via La Masa 34, 20156, Milan, Italy.
[2] Airbus Defence and Space GmbH, Rechliner Str., 85077 Manching, Germany.
[3] Airbus Defence and Space SAU, Paseo John Lennon, 28906 Getafe, Spain.

ABSTRACT

The aviation industry's current push to reduce emissions has sparked interest in highly integrated hybrid-electric aircraft. Distributed electric propulsion (DEP) systems show promise in helping achieve these emission targets. However, the high integration of aircraft structure, aerodynamics, propulsion, and power supply in hybrid-electric DEP systems necessitates a multidisciplinary analysis approach to identify robust design trade-offs. This paper presents an extended multidisciplinary design and optimisation framework applied to a hybrid-electric regional aircraft configuration. The traditional aerostructural optimization process has been enhanced to include aircraft stability and control aspects. To balance computational costs with accuracy of the optimization, a multi-fidelity approach is employed, utilizing both full-order and reduced-order models. An analytical model has been integrated to assess the flying qualities of the aircraft within the multidisciplinary framework. The results emphasize the critical role of accurate aerodynamic prediction models and the importance of incorporating flying qualities constraints during the optimsation of an aircraft desgin.

NOMENCLATURE

A_{cap} = wing caps area
$A_{stringer}$ = wing stringers area
b = wing semi-span
c = wing chord @root
$\bar{c}$ = wing mean chord
c_s = specific fuel consumption
C_j = aerodynamic coefficient
C_l = sectional lift coefficient
C_m = pitching moment coefficient
C_p = pressure coefficient
C_X = X-force coefficient
C_Z = Z-force coefficient
D = Aircraft integral Drag
F_X = X-Force in body axes
F_Z = Z-Force in body axes
L = aircraft integral Lift
$\vec{m}_{vec}$ = aircraft mass vector (mass, CG and inertia)
m_{wing} = wing mass
m_Y = pitching moment in body axes
q = pitch rate
R = aircraft range
R^2 = coefficient of determination
R_e = regressor relative error
RFC = reserve factor in compression
RFT = reserve factor in tension
$S.M.$ = aircraft static stability margin
U = Freestream velocity
V_Z = flowfield velocity Z-component in aircraft axes
W = aircraft weight
x_{CG} = aircraft center of gravity long. coordinate
x_{NP} = aircraft neutral point long. coordinate
y_{kink} = wing kink y-coordinate
y_{eprop} = wing electric propellers y-coordinate
α = angle of attack
δ_e = elevator angle position
$\theta_{electric}$ = electric rotor blade pitch angle
θ_{hybrid} = hybrid rotor pitch angle
ω_{sp} = aircraft short period mode frequency
ζ_{sp} = aircraft short period mode damping
ζ_{ph} = aircraft phugoid mode damping

Copyright Statement
The authors confirm that they, and/or their company or organization, hold copyright on all of the original material included in this paper. The authors also confirm that they have obtained permission, from the copyright holder of any third-party material included in this paper, to publish it as part of their paper. The authors confirm that they give permission, or have obtained permission from the copyright holder of this paper, for the publication and distribution of this paper as part of the ERF proceedings or as individual offprints from the proceedings and for inclusion in a freely accessible web-based repository.

INTRODUCTION

In recent years, there has been a growing interest on directing technological development towards environmentally compliant solutions. This effort includes optimizing existing traditional technologies to maintain, or even enhance, performance while simultaneously minimizing environmental impact. In this context, the aerospace sector has also seen a strong push toward the development of low-emission technologies.

Within regional aviation, there has also been growing interest in reducing emissions while maximizing performance. Within the Clean Aviation framework, the Hybrid-Electric Regional Architecture (HERA) project has been developed to investigate and optimize the concept of a regional aircraft integrating hybrid-electric technologies. HERA aims to identify and assess viable aircraft-level architectures capable of meeting the -50% greenhouse gas (GHG) emission target outlined in the Strategic Research and Innovation Agenda (SRIA). With a capacity of approximately 50–100 seats and a range suited to routes up to 1000 km, the aircraft is expected to enter into service by the 2040s. It will be compatible with multimodal transportation frameworks and powered by hybrid-electric systems combining batteries or fuel cells with Sustainable Aviation Fuel (SAF) or hydrogen combustion. This architecture is expected to reduce emissions by up to 90% while fully complying with ICAO noise regulations. Figure 1 shows a conceptual representation of the HERA aircraft.

Figure 1. HERA conceptual design representation.

One of HERA's use cases distinguishing features is the use of distributed electric propulsion (DEP), where multiple propellers, both hybrid and electric, are placed along the wing span. This setup not only can possibly modify aerodynamic performance, but also improves safety through propulsion redundancy. However, implementing such a configuration introduces significant engineering challenges. Important among these are the aerodynamic interactions between the wing and propellers, which strongly affect the wing's performance and overall efficiency, while introducing sensitivity on the design variables related to propeller geometry.

Numerous studies in literature have highlighted the non-negligible effects of propeller–wing and propeller–propeller interactions on the aerodynamic performance of innovative aircraft configurations, as a function of the design variables. These effects include rotor-induced downwash, variations in local dynamic pressure, and upwash/downwash regions that depend on the rotor's rotation direction, all of which significantly alter the wing's load distribution, while at the same time, the wing induces a thickness and a doublet induced velocity along the propeller disk (Ref. 1). At Politecnico di Milano, extensive research has been conducted to experimentally and numerically to quantify these aerodynamic interactions with respect to different design variables (Refs. 2–4). Geng et al. also studied the performance implications of wingtip-mounted and distributed propellers using the HMB3 CFD solver (Ref. 5). Their results indicate that these interactions consistently influence both propeller and wing performance, and thus must be carefully accounted for during the design phase.

Additionally, hybrid-electric configurations like HERA require a highly multidisciplinary design approach from the earliest stages of development. This includes not only aerodynamic and structural aspects, but also propulsion, acoustics, and safety and certification requirements.

A multidisciplinary framework, indeed, enables the use of discipline-based objective functions such as the aircraft aerodynamic L/D ratio, and the wing structural mass, quantities that are directly linked to the overall manufacturing and operational costs of the aircraft. Optimizing these different quantities is essential to ensure affordability, a critical success factor for new aerospace products. Moreover, within the design of new hybrid-electric DEP configurations, where the interdependency of the aircraft systems is more complex than conventional configurations, a multidisciplinary approach is essential to realize optimal feasible designs.

Affordability is further influenced by certification requirements and social acceptance. Certification is often among the most costly and time-consuming phases of aircraft development, and meeting safety standards involves extensive testing, validation, and sometimes multiple design iterations driven by regulatory feedback. These iterations increase development costs and delay the time to market of new aircraft, making it advantageous to consider certification requirements such as flying qualities constraints already in the preliminary design phase to improve the overall feasibility of the new configuration.

Given the complexity of the design space, Multidisciplinary Design Optimization (MDO) is a well-suited approach for the development of such integrated aircraft. Several works in literature have applied MDO in the early stages of aircraft development to explore feasible and compliant design regions. Hendricks et al. (Ref. 6) proposed an MDO environment for preliminary eVTOL configurations, coupling different subsystems in the MDO formulation. Petersson et al. (Ref. 7) highlighted how feasible designs can be achieved under industrial constraints using MDO in both preliminary and conceptual phases, significantly reducing redesign costs. In this work, he presented MDO results for transonic swept-wing aerostructural design and fuselage optimization. Gazaix et al. (Ref. 8) applied MDO to the aerostructural design of an aircraft engine pylon, highlighting the multi-disciplinarity of the problem and the difficulties of integrating high-fidelity simulations to predict pylon loads.

For the purpose of efficiently populating the design space reduced order models can be considered. Frink et al. (Ref. 9). indeed employed surrogate models to represent the aerodynamic behavior of the SACCON configuration developed by the NATO RTO. Using a Kriging-based surrogate model built from stability and control derivatives, he accurately predicted dynamic responses gaining a significant advantage in terms of computational costs. Granata et al. (Ref. 10) proposed an alternative method using DUST aerodynamic solver to simulate multi-frequency oscillatory motions and estimating the complete set of stability derivatives. This enables comprehensive flight mechanics modeling and the inclusion of flying qualities constraints within the MDO framework.

The objective of the present work is therefore to perform a multi-disciplinary analysis based on detailed aerodynamic analysis of one of the HERA aircraft configuration, namely the Use Case 'B' (UCB), with a focus on wing–propeller interaction effects and their impact on design optimization. We investigate the usage of a multi-fidelity approach in that some of the models, i.e. aerodynamic and stability and control models, are also instantiated as surrogates of the corresponding full-order model. The multidisciplinary optimization environment is expanded to incorporate flying qualities constraints into the optimization loop. These are evaluated using the mid-fidelity aerodynamic solver DUST and constrains are created according to guidelines from certification requirements. The aircraft trim is also included in the loop. This framework allows to speed up the convergence towards a feasible design space, optimized configuration, thus potentially reducing the need for costly redesigns in later development stages. Finally, this study also evaluates the impact of using surrogate discipline models for multidisciplinary design optimization. The developed framework leverages the DUST (Ref. 11) aerodynamic solver and the open-source optimizer GEMSEO (Ref. 12):

- *DUST* is a mid-fidelity aerodynamic computational tool, developed by Politecnico di Milano, which provides a fast and reliable simulation environment for complex aircraft configurations, such as eVTOL aircraft, tiltrotors and DEP configurations. DUST is an open-source code released under the MIT license, integrating different aerodynamic models for solid bodies, thick surface panels, thin vortex lattice elements, and lifting line elements. Additionally, a Vortex Particle Method (VPM) is implemented for wake modeling, offering a stable Lagrangian representation of free-vorticity flow fields. This feature makes it particularly suitable for numerical simulations of configurations with strong aerodynamic interactions. Details regarding the solver's mathematical formulation can be found in (Ref. 13). In this study, DUST is used to develop the aerodynamic model of the HERA aircraft and to perform aerodynamic analyses, including polar curves, stability and control assessments, and wake interaction aerodynamics studies.

- *GEMSEO* (Generic Engine for Multidisciplinary Scenarios, Exploration, and Optimization) is an open-source Python-based software designed to automate multidisciplinary processes, particularly those related to Multidisciplinary Design Optimization (MDO). It offers a variety of MDO formulations and is built on NumPy, SciPy, and Matplotlib, incorporating algorithms for coupling, design of experiments, linear problems, optimization, machine learning, surrogate modeling, uncertainty quantification, and visualization. GEMSEO can be integrated into simulation platforms or used as a standalone tool. It supports Python, MATLAB, Scilab scripts, Excel spreadsheets, and other executable codes callable from Python.

NUMERICAL METHODOLOGY

HERA DUST Numerical Model

This section describes the aerodynamic model built in DUST, developed for HERA. This model, cross-validated against RANS solutions of the TAU software based on the Spalart-Allmaras turbulence model (Ref. 14), was employed for the aerodynamic analysis of the configuration and a reduced vortex-lattice (VL) version is used in the MDO loop for configuration optimization. Specifically, DUST was employed for load estimation and for evaluating aerodynamic stability properties, which were used to compute the flying qualities of the aircraft. For these reasons, the DUST model represents an important element of the present work and is described in detail in the following.

The HERA configuration features a main wing and a T-tail horizontal stabilizer. It also incorporates an innovative hybrid-electric propulsion system, with propulsion units mounted on the main wing. In particular, each wing hosts one hybrid rotor placed near the wing root, and two smaller electric rotors positioned farther outboard. Depending on the flight regime, the thrust distribution between the hybrid and electric motors varies.

Figure 2 shows the aerodynamic model of HERA built in DUST, which consists of 14460 mesh elements, along with the body axes orientation employed in the present work. The main wing, horizontal tail, and vertical tail were parametrically generated in DUST and modeled using surface panel (SP) elements. A complete analytical description of the formulation for these implicit elements can be found in Ref. (Ref. 13). The full parametrization of these components was chosen due to its suitability for use within a multidisciplinary optimizer. Control surfaces were also modeled on each of these lifting surfaces, leveraging the built-in capabilities provided in DUST (Ref. 15). The fuselage is likewise represented with surface panel elements. Its mesh was generated externally using a MATLAB script, based on the parametric fuselage modeling formulation described in (Ref. 16). The structured mesh is then imported into DUST using raw point and connectivity files. The rotors, on the other hand, were modeled using lifting-line elements (Ref. 13), which enable solving an explicit problem by evaluating blade loads through the use of C81 lookup tables. The lookup tables for both hybrid and electric rotor blades were generated using the open-source tool NeuralFoil by Peter Sharpe (Ref. 17), a rapid airfoil analysis tool based on a hybrid approach that combines physics-informed machine learning techniques with analytical models, trained on tens of millions of XFoil simulations. For all aerodynamic components, parasite drag, not captured

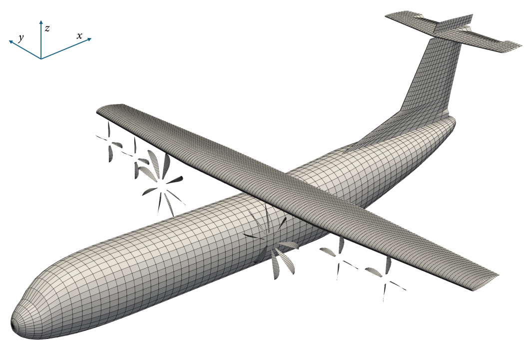

Figure 2. HERA DUST Aerodynamic mesh and body axes orientation.

by the mid-fidelity aerodynamic solver, is considered within the optimizations as an assumed constant value.

Table 1 reports the number of elements in the mesh for each component of the model, for both the surface panel model and the reduced vortex lattice model. The mesh resolution was chosen following a convergence study for each part of the aerodynamic model, ensuring that load variation remained within 0.5%. For the static simulations, used both for validation and for assessing the aircraft's static stability, a total simulation time of 0.3 seconds was chosen, with a time step of 0.001 seconds. For the dynamic simulations, the simulation time was set to 1 second, due to the need to capture the dynamic motions described in (Ref. 10).

Table 1. Aerodynamic mesh specifications (Vortex Lattice model in brackets)

Solver	N.Components	N.elements x comp.
Wing	**1**	9000 (600)
Tail	**1**	2080 (400)
Hybrid Rotor	**2**	232 (144)
Electric Rotor	**4**	116 (72)
Fuselage	**1**	2452 (/)
Total	**/**	14460 (1216)

Table 2 instead lists the aerodynamic conditions considered for the multi-fidelity validation of the model against the TAU solver. For optimization purposes, only cruise flight conditions will be considered. Aerodynamic coefficients were computed with respect to dynamic pressure and the geometric properties of the aircraft as non-dimensional.

Table 2. Angle of Attack per Solver and Condition

Solver	Condition	Angle of Attack [°]
DUST	**Cruise**	0, 5, 10
TAU	**Cruise**	0, 5, 10

The model described above was used to perform cross-validation with a CFD model of HERA, specifically characterized by the presence of actuator disks for the modeling of the propellers. The actuator disks in the CFD model take as input the loads provided by DUST, ensuring that the validation of the wing loading is carried out under equal propeller thrust conditions. The focus of this part of the work is indeed on the accurate characterization of the loads acting on the wing, including those due to wing–propeller interaction, which is essential for the subsequent optimization of the configuration.

Following validation and aerodynamic analysis, the DUST model is then replaced with a lower-fidelity DUST model characterized by Vortex Lattice elements (Tab. 1 shows the mesh specification in brackets) instead of the more computationally expensive 3D surface panel elements. The Vortex Lattice model was correlated with the surface panel model, as will be shown in Figure 11, and then used in the MDO loop. This allowed for a computational cost speed-up of up to 10 times compared to the surface panel model, which was critical during the testing phase of the implemented code.

Multidisciplinary Optimization Framework

This section presents the multidisciplinary optimization environment developed and used in this work to perform MDO on the HERA configuration. The framework has been developed in previous works (Ref. 18)- (Ref. 19) at Airbus Defence and Space and has been further extended and refined in the present study to achieve the objectives outlined in the introduction. The following describes the developed environment and the logic behind the implementation of the tool, along with recent additions introduced in this work. The MDO framework is based on the need to couple various disciplines that reflect different physical aspects involved in the flight physics of the aircraft. In this regard, the open-source optimizer GEMSEO proves to be well-suited, as it is specifically designed to connect multiple disciplines. Through a customized library, it enables the communication between different design variables linked to various aircraft components. The framework itself is composed of several modules interfacing with GEMSEO and coordinated by an executable script that also includes the optimization logic, chosen by the user among the available strategies in GEMSEO.

- The assembly module acts as a descriptive layer that connects the flight environment (i.e., mission segment or flight condition under analysis) with the physical components of the aircraft. This module includes all the classes needed to define subsystems, introduced as objects with attributes (defining their properties) and methods (for operating on the physical components). For example, one such class is Section, a dictionary containing all the information about each airfoil profile of a parametric Wing class (another object in the assembly). The definition and interconnection of these subsystems follow the CPACS convention (Ref. 20), ensuring proper handling of components linked by interaction constraints (e.g., geometrical dependencies). By chaining simpler elements, the full system is defined. Complex components can be nested and retain data relevant to their hierarchical level, for instance, a propeller composed of

identical blades, each defined by sections placed according to chord and twist distribution, as illustrated in Fig. 3
.

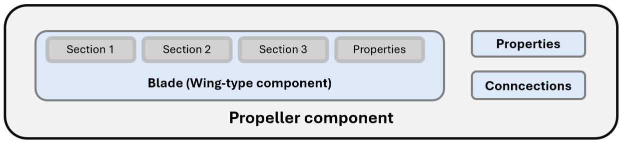

Figure 3. Data structure of a propeller component.

- Disciplines represent independent physical models such as aerodynamics or structural analysis. To be integrated into the GEMSEO workflow, each discipline must expose an interface specifying its required input variables and the output it generates. In other words, each discipline is implemented as a dedicated module containing the classes needed to retrieve inputs from the assembly components and deliver pre-defined outputs compatible with GEMSEO. These outputs can then be used as objective functions or constraints in the optimization process. The disciplines developed and used in this work focus on the aero-structural optimization of HERA's main wing, also considering flying qualities constraints:

  Aeordynamics: The aerodynamic module serves as the interface to the mid-fidelity aerodynamic code DUST. It takes input from the assembly module, thus having full knowledge of the aircraft components and flight conditions. With these inputs, the aerodynamic problem is uniquely defined in DUST, including parametric geometry generation (wings, fuselage, propeller) and flight conditions (freestream velocity, angle of attack and sideslip). Users may also select specific options such as simulation timestep, total simulated time, mesh resolution, number of wake panels, and vortex particles. Beyond static aerodynamics, the module implements subroutines for computing aerodynamic stability and control derivatives. These include static derivatives (evaluated via finite differences between two attitudes), dynamic stability derivatives (computed with the methods from (Ref. 10)), and control derivatives for aileron, elevator, and rudder, also evaluated using finite differences. Derivatives are used by the stability and control discipline for the reduced-order modeling of the vehicle. The final aerodynamic outputs include aerodynamic loads (lift, drag, thrust, moments) and all stability/control derivatives.

  Structural Sizing: the structural sizing discipline aims at sizing the primary wing structure, while the structure of the fuselage is kept constant as well as that of the tail plane. The model sizes the wing spars, stringers, ribs and panels by using spanwise aerodynamic loads, the weight and position of the engines. The structural sizing model defines the set of thicknesses that minimize the weight for each section using different criteria for each skin and web, maintaining a predefined reserve factor (RF) of 1.5 which are implemented in the Airbus inhouse mid-fidelity structual sizing tool AMPET (Ref. 21) and more recently coupled by the in-house multidisciplinary framework built around GEMSEO (Ref. 22)

  Weight and Balance: the weight and balance module handles the aggregation of mass properties of all aircraft components. Each component is assigned a mass, center of gravity, and inertia tensor, either user-defined or computed by another discipline (e.g., structural sizing for the wing). The module sums the masses, computes the global center of gravity, and calculates the total inertia tensor in body axes. This information is then used by the stability and control discipline.

  Stability and Control: the stability and control module gathers aerodynamic derivatives and inertial data to compute three different kind of outputs: static margin (SM), flying qualities (based on the reduced formulation from (Ref. 23)), and, if desired, maneuvering time estimates based on control surface inputs and known damping/control derivatives and inertial properties. Generally speaking, this discipline provides essential metrics for assessing vehicle handling and stability.

The *Variable* class represents the final key element of the framework. It allows specific attributes to be flagged as optimization variables. Each variable is a simple structure storing a name, initial value, and optional bounds. Variables are defined in the main executable, and they are attached to the components of the assembly. Once attached to a component attribute, the optimizer can track and update it throughout the optimization.

Within GEMSEO, several MDO formulations are available to couple the MDA analysis and the optimization logic, such as: the Multidisciplinary Feasible (MDF), which solves the coupled system at each optimization iteration ensuring feasibility; the Individual Discipline Feasible (IDF), which treats coupling variables as independent optimization variables with consistency constraints; and the Bi-Level formulation, which separates the problem into a lower-level disciplinary optimization and an upper-level coordination problem. Figure 4 illustrates a high-level diagram of the optimization process and interactions between the various components of the framework, using the MDF (Multidisciplinary Feasible) algorithm.

Surrogate modelling

The presented problem involve multiple disciplines and, as in the case of DUST, requires executing simulations from dedicated solvers. During an optimization process, this becomes particularly onerous due to the need to repeatedly perform the simulation while varying design parameters and so computing the Jacobian matrix that supplies sensitivity information to the optimization algorithm (Fig. 4). This process results in significant computational costs, provided that a finite difference approach must be used for DUST during the optimisation.

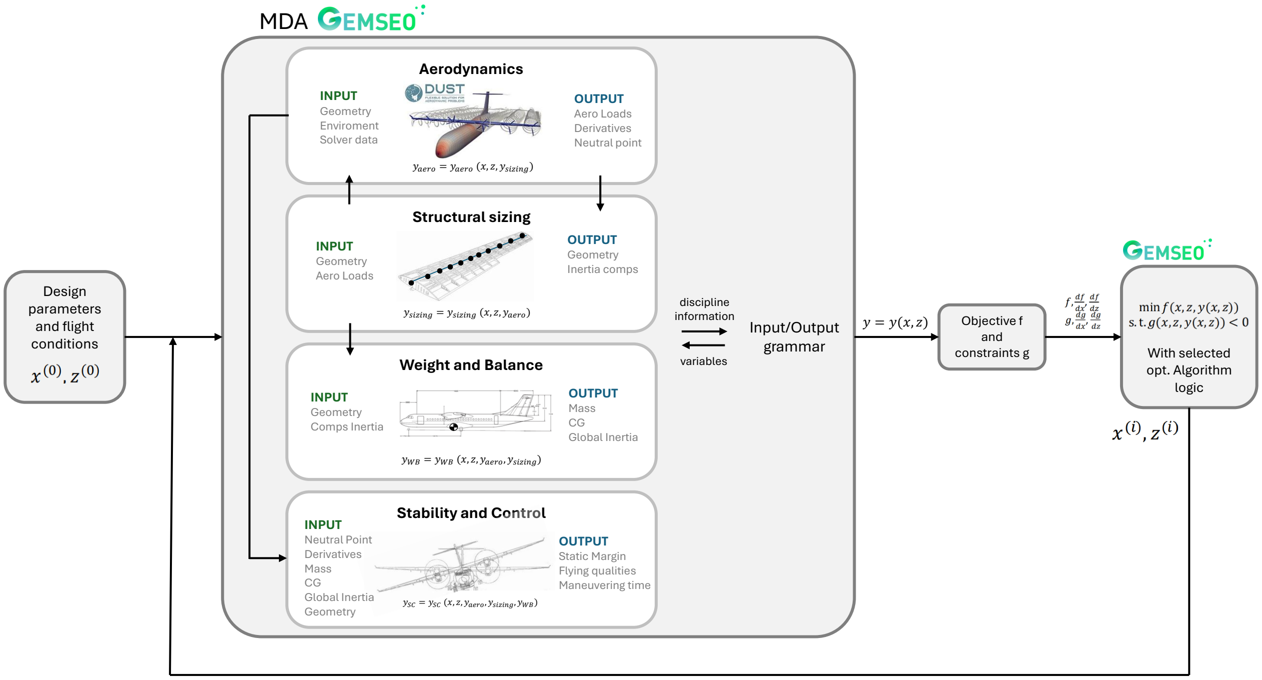

Figure 4. DUST-GEMSEO interface and optimization loop with Multidisciplinary Feasible (MDF) MDO formulation architecture.

To alleviate this issue, the adoption of surrogate models, constructed through Design of Experiment (DOE) approaches, has proven highly effective, as supported by recent literature (Ref. 24) (Ref. 25). A surrogate model approximates a given discipline as an explicit Multi-Input Multi-Output (MIMO) function of the design variables involved in the optimization (Ref. 26).

These models are built using a DOE (Design of Experiment) approach. The DOE implemented in the framework can be divided into five significant steps.

- *Planning* The first step is the planning the experiment and so, the definition of the discipline I/O (Input/Output) Grammar, hence the design space and the constraints.
- *Sampling* The second step consists of selecting a sampling strategy to choose a set of meaningful points within the design space that will serve as inputs for evaluating the discipline. GEMSEO provides several sampling methods for this purpose, such as the FFS (Full Factorial Sampling), LHS (Latin Hypercube Sampling), and quasi-random sequences such as Sobol and Halton or simpler Monte Carlo.
- *Execution* The third step concerns the actual execution of the experiment, where the disciplinary solver is run on each of the sampled points selected in the previous phase, and the outputs of the discipline are stored.
- *Regression* The fourth step involves building the surrogate Input/Output model. This is done by training a regression model that approximate the relationship between the design variables and the outputs of the discipline. GEMSEO supports various supervised Machine Learning (ML) models for this task. Linear regression is often used for its simplicity and speed in capturing basic trends, while polynomial regression is useful for modeling nonlinear behavior. More advanced techniques include Gaussian Process Regression (GPR or Kriging), which provides both predictions and uncertainty estimates and is well-suited for smooth nonlinear functions. Radial Basis Function (RBF) regressor is also available and effective for scattered, nonlinear data.
- *Validation* Finally, in the fifth step, the generated model is validated by assessing its accuracy through a comparison between the model and the output of the original discipline. The validation points can be taken from the sampling dataset using different strategies (such as manual split, leave-one-out, or K-fold (Ref. 12)) or generated on a new set of points. To evaluate the performance of the resulting model on the validation points, several indices are widely used in the literature, such as the R^2 and the relative error R_e (Ref. 12). Indices are defined as:

$$R^2 = 1 - \frac{\sum_i (\hat{y}_i - y_i)^2}{\sum_i (y_i - \bar{y})^2}, \quad R_e = ||\frac{\hat{\mathbf{y}} - \mathbf{y}}{\mathbf{y}}|| \tag{1}$$

where $\hat{\mathbf{y}}$ is the model evaluated at the validation points, and $\mathbf{y}$ is the output of the original discipline at the validation points.

A dedicated module has been developed within the multidisciplinary framework to create surrogate models via DOE approach. Each disciplinary block in Figure 4 is treated as a black box with its own input/output structure, and GEMSEO's built-in algorithms are employed for both sampling and model fitting. When the surrogate option is activated, the original block is replaced by a MIMO surrogate that preserves the same I/O structure, emulating the behavior of the original discipline with significantly reduced computational effort.

In the present work, the module was used to create surrogate models for the aerodynamic loads and stability discipline (see Fig. 4), which is characterized by the use of DUST. DUST samples are selected using Latin Hypercube Sampling (LHS), a statistical method for generating a near-random sample of parameter values from a multidimensional distribution and aims to spread the sample points more evenly across all possible values. Also, GPR and RBF regressor are used to generate the surrogate models from the DOE points.

RESULTS

This section addresses two main topics. The first concerns the validation of the DUST aerodynamic model against the RANS-based solutions of the TAU solver. The aerodynamic interaction between the wing and the propellers will be analyzed in terms of its effects on the wing loads, which are central to the configuration optimization process.

Then, the optimization will be carried out. This part is divided into three steps: the transition to a reduced vortex lattice model, the creation of surrogate models, and finally, the optimization process. The optimization process is further split in two main phases: (i) a trim optimization, aimed at identifying the steady-state cruise attitude using the MDO framework (ii) the actual optimization of the geometry and propeller placement under cruise trim conditions, considering constraints on stability derivatives and flying qualities. These last two phases could technically have been combined, as the developed MDO framework supports trim-in-the-loop optimization. However, they were separated to reduce the surrogate model training cost, which would have been higher in a fully coupled setup. Moreover, as this study was part of the testing phase of the implemented framework, the decoupled approach allowed for more controlled validation. Trim-in-the-loop integration will be object of future works.

Aerodynamic analysis

This paragraph analyzes the cross-validation between the DUST model and the TAU CFD model, as well as the aerodynamic interaction effects between the wing and the propellers. Figure 5 shows a comparison of the pressure distribution between the DUST model on the left and the TAU model on the right. As previously discussed, the TAU model includes actuator disks to simulate the propellers, whereas DUST employs lifting line elements. The main goal of this phase is to observe the behavior of the two models and ensure that a consistent setup is being established. As shown in Figure 5 (a), for an angle of attack $\alpha = 0°$, the correlation between the two aerodynamic solvers is good, although the CFD solver, likely due to the use of actuator disks and mesh dissipation, exhibits a more limited interaction effect on the wing. A similar observation can be made for Figure 5 (b), corresponding to $\alpha = 5°$. At $\alpha = 10°$, it is evident that DUST predicts stronger interaction effects, as seen from the larger spanwise deviation of C_p. However, it fails to capture flow separation effects caused by the high angle of attack under cruise conditions. This separation leads to a reduction in aerodynamic load that the VPM solver is not able to accurately reproduce in this higher attitude of the aircraft.

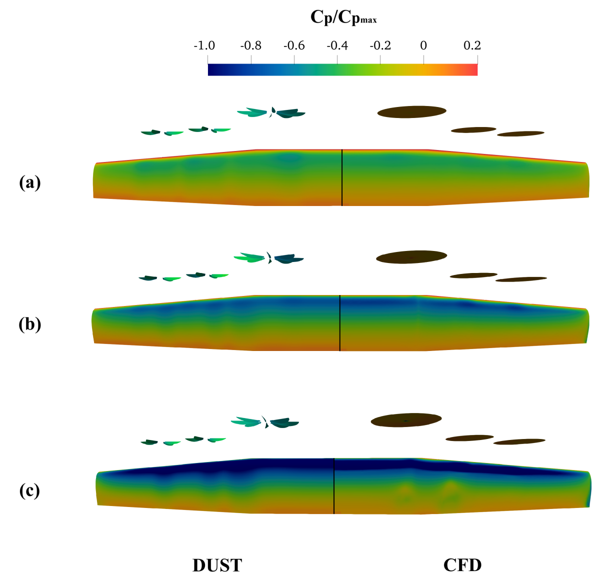

Figure 5. Pressure coefficient distribution on the wing for DUST and TAU (CFD RANS) solutions (a) $\alpha = 0°$ **(b)** $\alpha = 5°$ **(c)** $\alpha = 10°$

Figure 6 shows the chordwise distribution of C_p for angles of attack $\alpha = 0°, 5°, 10°$, at two different spanwise sections: one located within the propeller wake (in-wake, $y/b = 0.2985$), and one outside the propeller wake (out-wake, $y/b = 0.9630$). It can be observed that for angles $\alpha = 0°$ and $5°$, there is excellent agreement between the models both in-wake and out-wake. However, for $\alpha = 10°$, DUST accurately captures the out-wake section but fails in the in-wake region. This discrepancy is due to the fact that, in the in-wake region, the propeller wake induces an upwash and increases the dynamic pressure on the wing, triggering flow separation, an effect already visible in Figure 5. In Figure 6 (f), this separation manifests as a sudden drop in C_p, which results in a significant decrease in wing loading in the in-wake region.

Figure 7 shows the comparison between DUST and TAU in terms of the spanwise lift distribution for different angles of attack $\alpha = 0, 5, 10°$. A slight overestimation of the load by TAU compared to DUST can be observed, but overall the correlation is excellent for the first two angles of attack, particularly in terms of the trend and the spanwise derivative of the

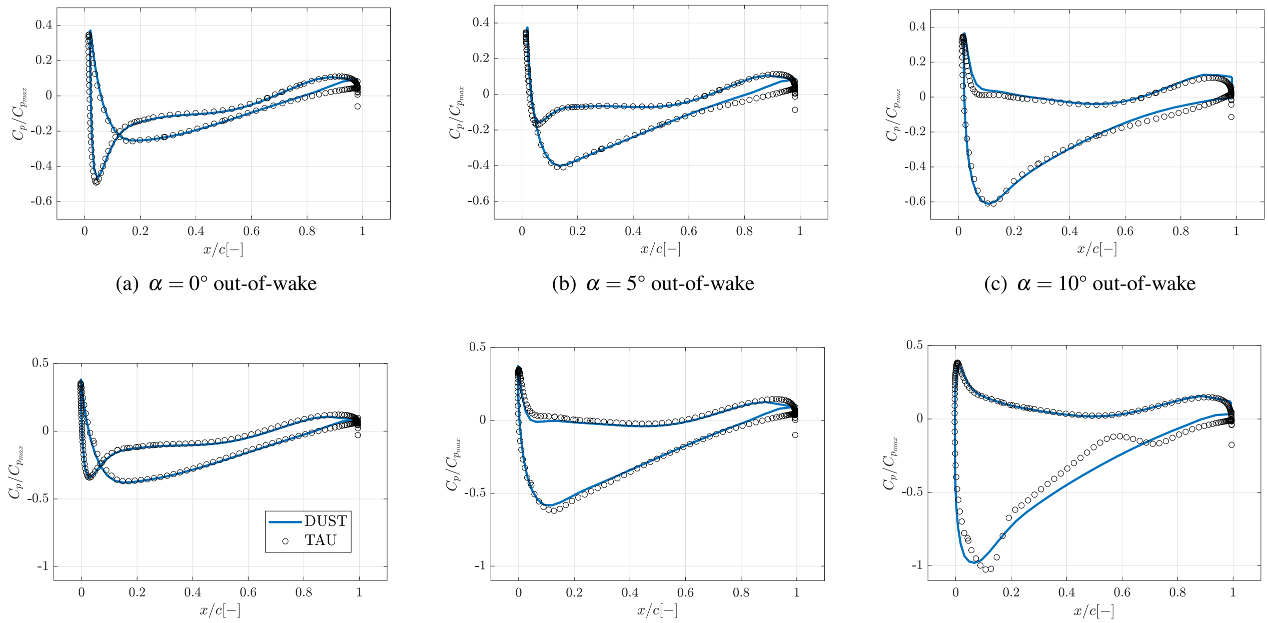

(a) $\alpha = 0°$ out-of-wake (b) $\alpha = 5°$ out-of-wake (c) $\alpha = 10°$ out-of-wake

(d) $\alpha = 0°$ in-wake (e) $\alpha = 5°$ in-wake (f) $\alpha = 10°$ in-wake

Figure 6. Chordwise pressure coefficient distribution, non-dimensionalized with respect to the maximum value, for different angles of attack, inside (in-wake: $y/b = 0.31$) and outside (out-of-wake: $y/b = 0.96$) the propeller wake, DUST and TAU solutions.

load. At $\alpha = 10°$, separation effects captured by the CFD solver become significant, leading to noticeable differences in the load distribution. In fact, DUST overestimates the load by approximately 10%, highlighting the limitations of the VPM solver at high angles of attack. It is important to note that the largest discrepancy occurs around $y/b = 0.4$, where the wing–propeller interaction induces flow separation.

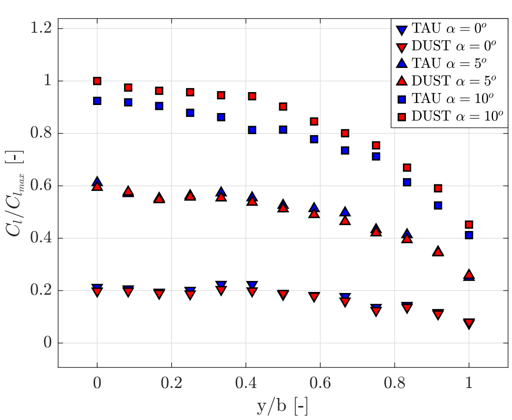

Figure 7. Sectional lift load coefficient as a function of the wing spanwise coordinate, for different angle of attacks, DUST and TAU solutions.

Similar considerations apply to the integral loads, shown in Figure 8 in terms of vertical force coefficient C_Z, longitudinal force coefficient C_X, and pitching moment coefficient C_m. In this representation, prior to the onset of stall at $\alpha = 10°$, there is excellent agreement between the models, especially for the derivatives C_{Z_α} and C_{m_α} (i.e., the slope of the curve between 0° and 5°), which deviate by less than 1% from TAU results. These derivatives are crucial both for the computation of flying qualities (such as static margin and the frequencies and damping of the aircraft's modes) and for the gradient-based optimization process. More over, addressing the L/D ratio for the conditions tested, a deviation between DUST and TAU of less then 5% is observed.

Figure 9 (a) presents a DUST-only comparison between the "Clean" configuration, i.e., the wing without propellers, and the configuration with propellers, for the three angles of attack previously analyzed. The effects of wing–propeller interaction on the spanwise loads can be clearly observed, leading to a characteristic upwash–downwash dipole pattern in the induced velocity field. This results in local variations in angle of attack and loading when the propeller wake impinges on the wing. This phenomenon is consistently observed across all three angles of attack and leads to variations in the integral loads of up to 10%, highlighting the importance of accounting for aerodynamic interactions in the optimization process.

Figure 9 (b) provides a visualization of the pressure coefficient (C_p) distribution over the wing, along with an iso-surface of vorticity based on the Q-criterion to represent the wake. This visualization reinforces the previously described effects: the main outcomes of the rotor–wing interaction are the increase in dynamic pressure, resulting in changes in C_p, and the presence of upwash and downwash caused by the propeller swirl, which is particularly pronounced for the hybrid rotor of HERA in cruise condition.

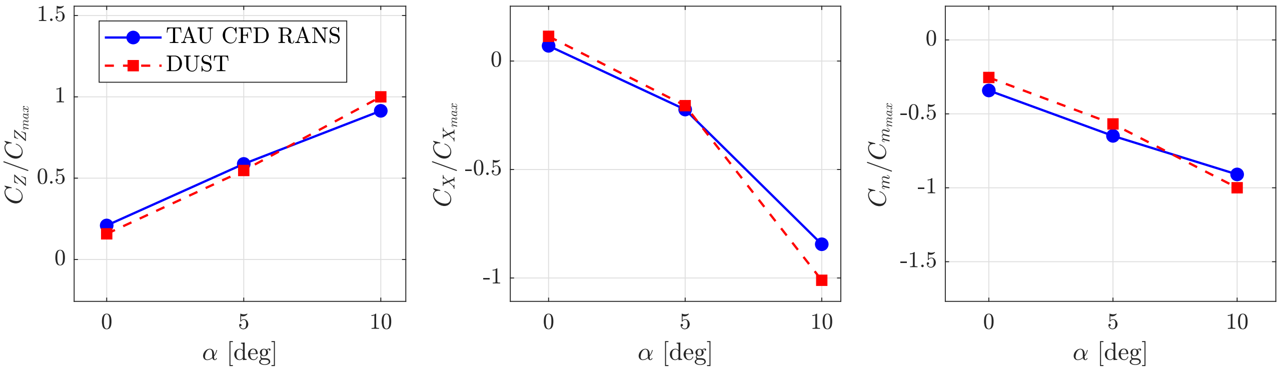

Figure 8. Integral loads force X and Y and pitching moment coefficient, comparison between DUST and TAU as a function of the angle of attack.

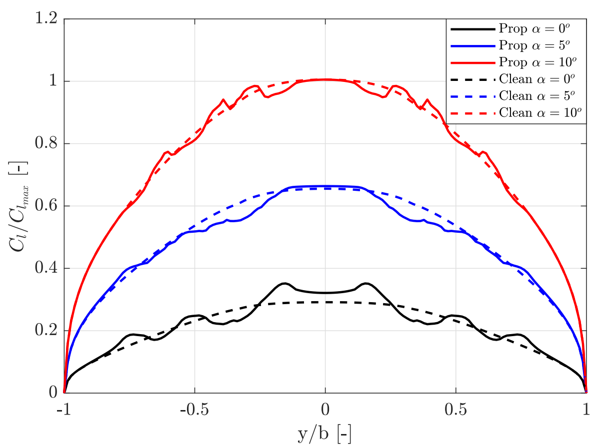

(a)

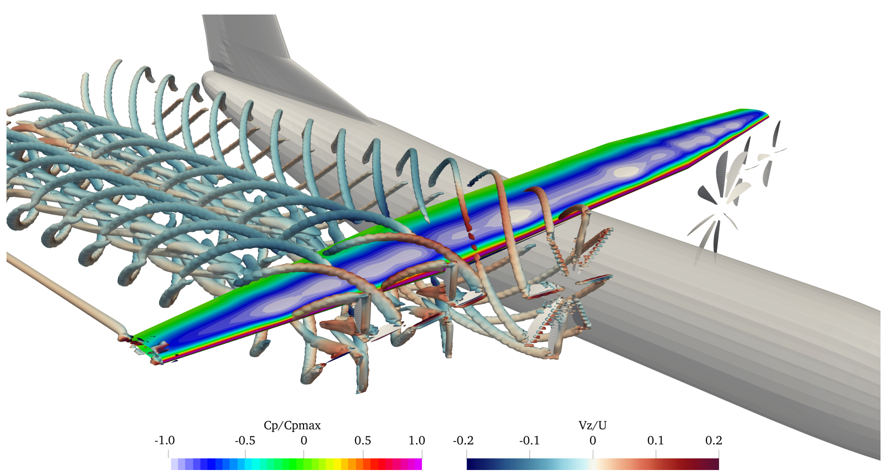

(b)

Figure 9. (a) DUST Sectional lift load coefficient as a function of the spanwise coordinate, for different angles of attack. Comparison between clean wing configuration and installed-propeller configuration. (b) DUST pressure coefficient distribution and flow visualization with three-dimensional vorticity iso-contours of Q-criterion.

Trim optimization

This section addresses the solution of the longitudinal trim problem for the previously introduced HERA configuration. In this context, the developed MDO framework optimizer is used to carry out the trim of the aircraft. Here, trim variables are treated as design variables subject to constraints.

Table 3 outlines the definition of the problem, showing that the considered trim variables are the aircraft angle of attack α, which primarily balances the vertical forces ($\sum F_Z$); the blade pitch of the hybrid and electric motors $\theta_{hybrid}, \theta_{electric}$, which contribute to the longitudinal trim ($\sum F_X$) by acting on the thrust of the rotors to counterbalance drag; and the deflection of the elevator control surface δ_e, which mainly balances the pitching moment around the center of gravity ($\sum m_{Y_{CG}}$). Since the number of trim variables exceeds the number of constraints, selecting different pitch values for the electric and hybrid propeller blades already provides insight into the optimal thrust split between the two propulsion types.

Figure 10 shows instead the Extended Design Structure Matrix (XDSM) of the trim problem, highlighting the input (vertical endings) and the output (horizontal) of each discipline, as well as the optimization loop path with the black line. The MDO forumlation is MDF. The optimizer chosen for the Trim solution is based on SLSQP (Sequential Least SQuares Programming) algorithm, a gradient-based method for solving nonlinear optimization problems with constraints, particularly effective when dealing with problems where both the objective function and the constraints are continuously differentiable.

Table 3. Trim Optimization problem definition

Trim Variables	Constraints	Objective
$-2^\circ < \alpha < 9^\circ$	$\sum F_X = 0$	L/D ratio
$40^\circ < \theta_{electric} < 60^\circ$	$\sum F_Z = 0$	
$40^\circ < \theta_{hybrid} < 60^\circ$	$\sum m_Y = 0$	
$-10^\circ < \delta_e < 10^\circ$		

Figure 11 shows the correlation between the DUST SP model, used in the previous section for the validation and analysis of wing, propeller aerodynamic interaction phenomena, and the DUST VL model, which is significantly less computationally expensive and therefore employed in the actual trim and MDO optimization process, including tests of optimizations without surrogate models. An excellent agreement can be observed between the two models in terms of sectional lift and drag, especially in terms of trend and derivative; these are two of the most critical quantities for an aero-structural optimization with trim, where the focus lies on maximizing L/D.

Concerning the surrogate discipline for the aerodynamic loads, figure 12 shows all the training points in the design space, along with slices of the surrogate model within the hypervolume of the design space, compared with validation points on the same slices. Slices are referred to the evaluation of the discipline on a input vector where only one design variable is varied. Table 4 displays the specifications of the surrogates for each output variable of the aerodynamic discipline, as well as the accuracy evaluation of each model in terms of coefficient of determination R^2 and relative error R_e. The surrogate was trained using the implemented DOE approach with LHS, a sampling technique designed to generate a uniformly distributed set of points within a Latin hypercube, enabling efficient exploration of the design parameter space. A total of 120 training points were used, a value selected after a convergence study on the number of samples needed to achieve a coefficient of determination R^2 of at least 0.9 for all involved quantities. The regression model employed to build the surrogate is a GPR regressor. A strong correspondence can be observed between the ML model and the validation points obtained from time-marching simulations, particularly in terms of trends and derivatives/gradients, thus enabling the optimization process to be carried out in a manner consistent with the full-order model. From Tab. 4 it can be observed that the linear trends (C_L, C_m) yield higher coefficients of determination and lower relative errors compared to the more complex trends of drag and thrust coefficients.

Table 4. Trim regression models and accuracy.

	C_L	C_D	C_m	C_t
n° samples	120	120	120	120
Regressor	GPR	GPR	GPR	GPR
R^2 [-]	0.9993	0.9757	0.9979	0.9580
R_e [%]	3.228	7.283	3.841	9.587

Figure 13 presents the results of the optimization: the trim condition, defined within a tolerance of 0.05 on the load coefficients, was achieved in 8 iterations. Figure 13 (a) shows the evolution of the total forces and moments acting on the aircraft across the optimization steps, confirming the convergence toward an equilibrium condition. Figure 13 (b) compares the outcomes of the trim optimization when performed with and without the surrogate model for the aerodynamic discipline. A strong correlation between the results is evident, demonstrating the validity and effectiveness of the DOE-based approach and the use of a surrogate model for optimization purposes.

Table 5 shows the computational times associated with each part of the described process. The comparison between trim without surrogates and trim with surrogate training reveals a time advantage of approximately 7%. It is important to highlight that this result is highly dependent on the type of analysis being performed, and that since the trim problem converges in only a few iterations, the benefit of using surrogates is limited. However, once the surrogate is generated, it becomes evident that the exploration of the design space is several orders of magnitude faster compared to using the original discipline.

Table 5. Trim computational time.

$t_{wo/surr}$	t_{train}	$t_{w/surr}$	$tot_{surrogate}$	$\%adv$
4h 34m	4h 16m	0m 1s	4h 16m	-6,57%

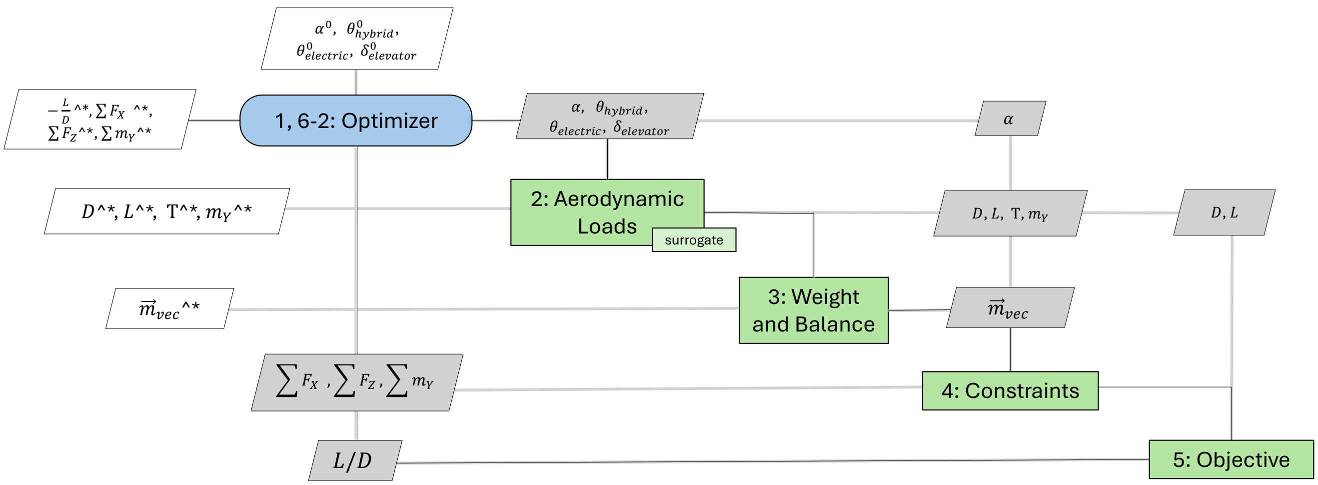

Figure 10. Extended Design Structure Matrix of the trim problem.

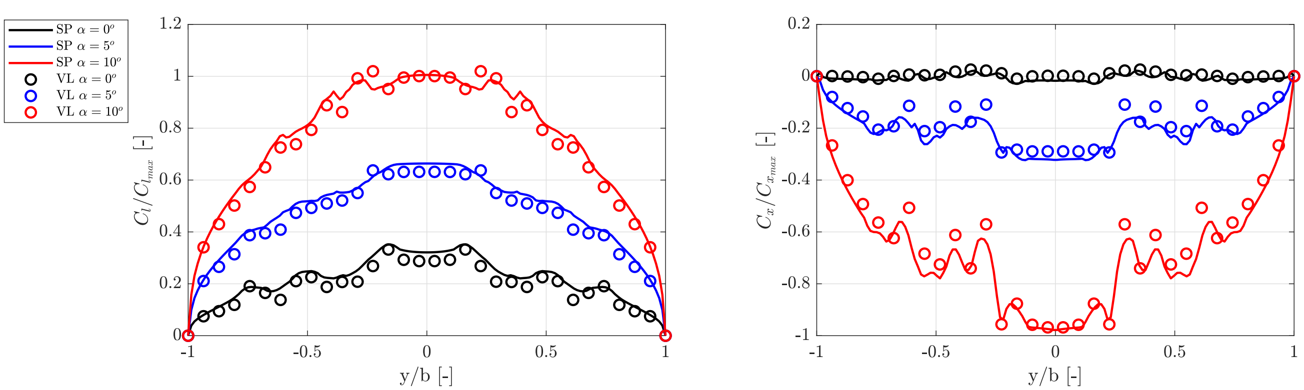

Figure 11. Spanwise wing sectional lift and drag coefficient as a function of the spanwise coordinate, comparison between DUST Surface Panel elements solution and Vortex Lattice elements

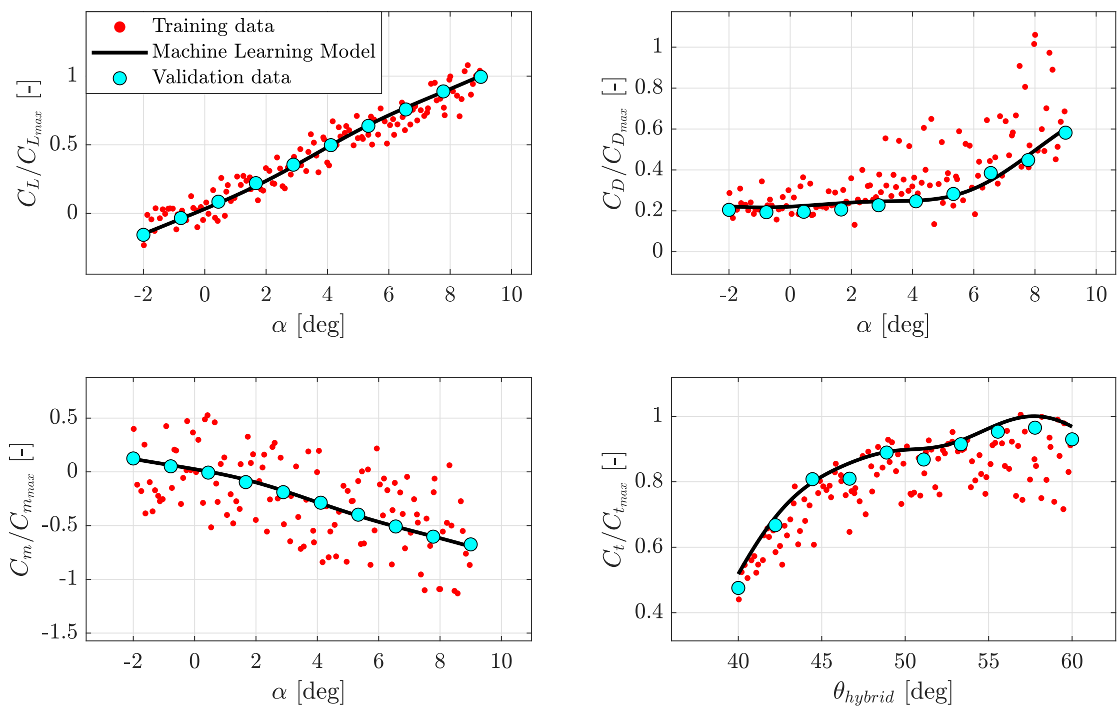

Figure 12. Slices of surrogate models for the aerodynamic discipline outputs. Training data (dependent on multiple variables), Surrogate data (slice), Validation points (slices).

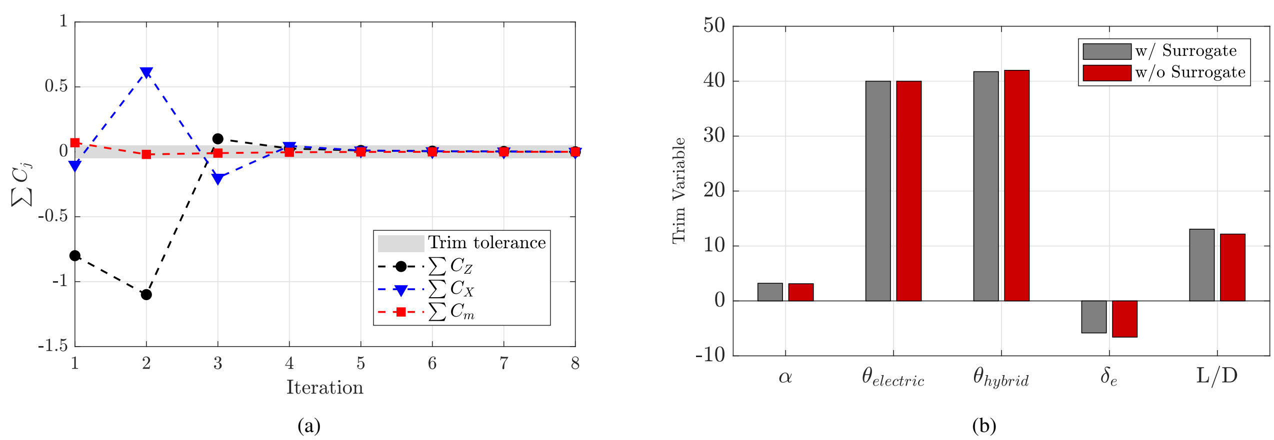

Figure 13. (a) Trim constraints evolution through the optimization (b) Trim optimization final results. Comparison between using the surrogate, and performing time-marching simulation through the optimization.

Multidisciplinary Design Optimization with Flying Qualities Constraints

This section presents the MDO performed on the HERA configuration. In this case we focus on two aspects: (i) analysing the effects of introducing or not surrogate models to evaluate the aerodynamic and stability and control behaviour (ii) the introduction of stability and control constraints in the optimisation. Table 6 outlines the definition of the optimization problem, specifically identifying the design variables, constraints, and the objective function. Among the design variables, four are purely geometric: the wing kink point y_{kink}; the wing tip twist θ_{tip} (twist varies linearly from the airfoil at the kink point); the position of the electric propellers y_{eprop}, which are translated along the wing span while maintaining a constant distance between them, as illustrated in Figure 14; finally, the horizontal tail plane scale is included in the optimization as a dedicated design parameter to actively control the stability and control characteristics of the aircraft, particularly in response to changes in mass and aerodynamics of the wing that influence the flight dynamics modes. In this context, where flying qualities constraints are incorporated into a multidisciplinary design framework, a global aircraft-level approach is essential, since the evaluation of the complete vehicle dynamics to ensure acceptable flight behavior across the design space is required. As an assumption of the problem, the wing component CG is considered fixed, even though its mass variation is accounted for the calculation of the global CG and in the evaluation of the flight dynamics properties. The remaining two design variables pertain to the wing structural geometry: the area of the caps at the wing root A_{cap} and the area of the stringers $A_{stringer}$. In addition to upper and lower bounds imposed on the design variables, the optimization includes constraints related to the aircraft's longitudinal FQ. From the perspective of static stability, a constraint is imposed on the aircraft's static margin, defined as:

$$S.M. = \frac{x_{\text{np}} - x_{\text{cg}}}{\bar{c}} = \frac{\frac{-\bar{c}C_{m\alpha}}{C_{Z\alpha}} - x_{\text{cg}}}{\bar{c}} = -\frac{C_{m_{CG\alpha}}}{C_{Z_{CG\alpha}}} \tag{2}$$

and required to lie between 5% and 35%, to ensure a good compromise between the aircraft's stability and maneuverability. Additional constraints relate to the dynamic behavior of the aircraft, including the damping and frequency of flight mechanincs mode (short period and phugoid), derived from a reduced-order model (Ref. 23) and the stability derivatives obtained using the methodology described in (Ref. 10). Employing the reference frame defined in Fig. 2, these constraints are defined as follows:

$$2\zeta_{sp}\omega_{sp} = -\left(\frac{m_{Y_q}}{I_y} - \frac{F_{Z_\alpha}}{Um} + \frac{m_{Y_\alpha}}{I_y}\right) \tag{3}$$

$$\omega_{sp} = \sqrt{-\frac{m_{Y_q}}{I_y}\frac{F_{Z_\alpha}}{Um} - \frac{m_{Y_\alpha}}{I_y}} \tag{4}$$

$$\zeta_{ph} = \frac{1}{\sqrt{2}}\frac{C_D}{C_L} \tag{5}$$

The objective of the optimization is to maximize the aircraft's range, defined by the Breguet range equation:

$$R = \frac{U}{c_s} \cdot \frac{L}{D} \cdot \ln\left(\frac{W_i}{W_f}\right) \tag{6}$$

which provides an optimal balance between maximizing the L/D ratio and minimizing the wing mass.

Table 6. MDO problem definition

Design Variables	Constraints	Objective
y_{kink}	$5 < S.M. < 35\%$	Range
θ_{tip}	$2.3 < \omega_{sp} < 3.5\ rad/s$	
y_{eprop}	$0.2 < \zeta_{sp} < 1.4$	
$A_{stringer}$@root	$\zeta_{ph} > 0.04$	
A_{cap}@root		
$htail\ scale$		

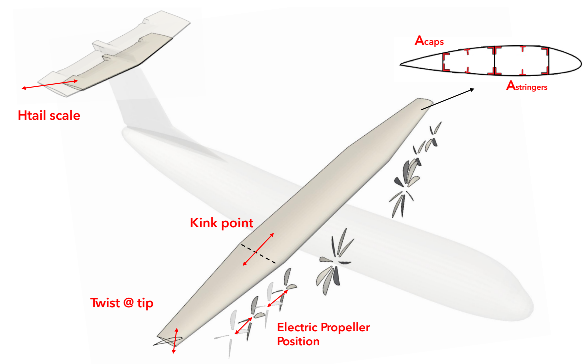

Figure 14. MDO problem geometric design variables scheme.

Figure 15 shows the XDSM diagram of the optimization problem, highlighting the inputs (vertical edges) and outputs (horizontal edges) of each discipline. The MDO forumlation is MDF. It is important to specify that the aerodynamic derivatives are computed in the aircraft's global reference frame, while the design synthesis discipline transport them to the aircraft's center of gravity, using the output provided by the weight and balance discipline. The optimizer chosen for the MDO solution is based on COBYLA (Constrained Optimization BY Linear Approximations) algorithm, a derivative-free optimization method designed for finding the minimum of a function subject to constraints, particularly useful when dealing with non-differentiable, constrained optimization problems.

Figure 16 shows the surrogate models generated by the developed framework, using RBF regressor for the aerodynamic loads discipline on 200 samples, and GPR regressor for the aerodynamic stability discipline on 120 samples. Table 7 displays the surrogates specification of each output variable, along with the coefficient of determination R^2 and the relative error R_e. From Figure 16 and Table 7, a strong correlation can be observed between the surrogate models generated for optimization and the validation points, both for the aerodynamic loads discipline and for the aerodynamic stability discipline. It can be noted that the aerodynamic loads discipline is characterized by lower gradients and greater data dispersion, due

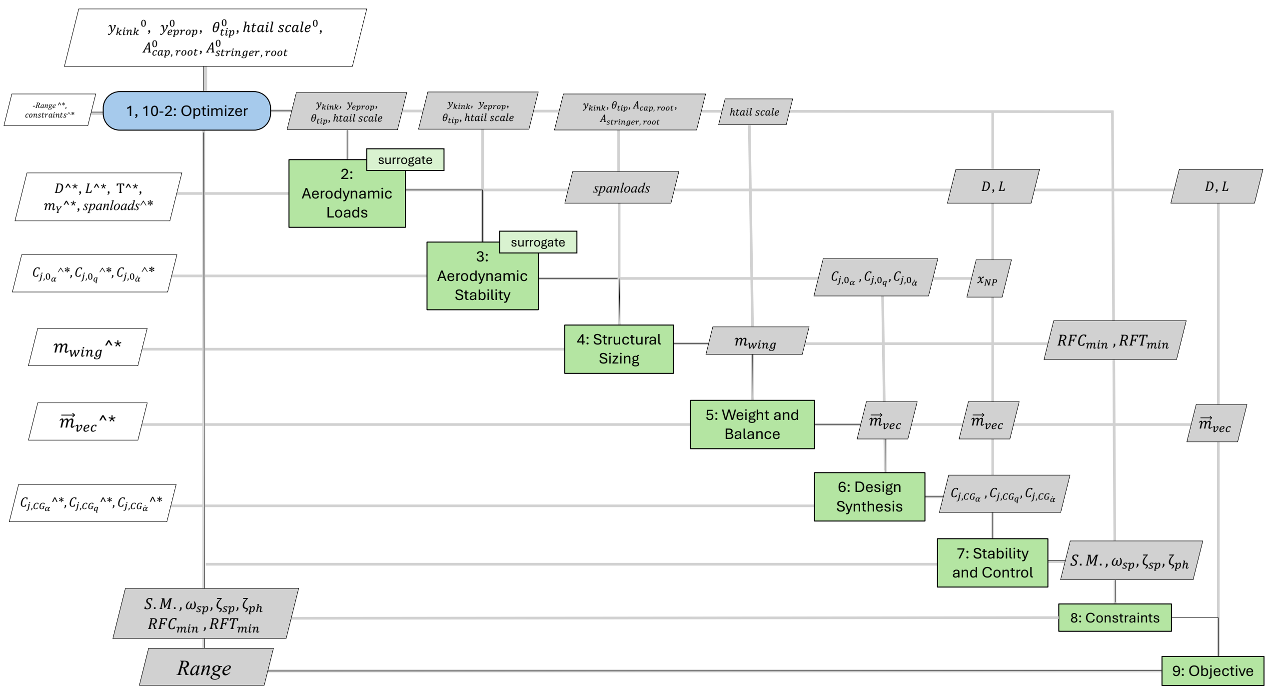

Figure 15. Extended Design Structure Matrix of the Optimization problem.

to the lower sensitivity of the coefficients C_L, C_D, and C_m with respect to the design variables. Despite this, all coefficients achieved R^2 scores greater than 0.97 and a mean R_e below 10%, as shown in Table 7. Regarding the surrogate models for the aerodynamic stability discipline, the dependence on the horizontal tail scale is dominant (Fig. 16, second row). This leads to a lower data dispersion and coefficients of determination R^2 higher than 0.99 (Table 7), due to the fact that the denominator of R^2 contains the mean of the validation data, despite relative errors being in line with those of the other models. Specifically, Figure 16 shows the trends of the aircraft neutral point x_{NP} and the dynamic stability derivatives $C_{m_{\dot{\alpha}}}$ and C_{m_q}, quantities computed by the DUST routine using the methodology described in (Ref. 10).

Table 7. Optimization regression models and accuracy.

	C_L	C_D	C_l	x_{NP}	$C_{m_{\dot{\alpha}}}$	C_{m_q}
$n°$ samples	200	200	200	125	125	125
Regressor	RBF	RBF	RBF	GPR	GPR	GPR
R^2 [-]	0.9804	0.9734	0.9841	0.9879	0.9981	0.9992
R_e [%]	3.229	9.452	4.842	8.981	7.470	4.628

Figure 18 shows the results of the MDO, in terms of design variables that satisfy the constraints on the flying qualities, and objectives. A good correlation can be observed between the results obtained with and without the surrogate model, highlighting the consistency of the DoE-based approach employed. In particular, Figure 18 (a) shows the results for the geometric and structural design variables of the optimization problem. The histogram is represented in terms of relative design space, meaning that a value of 0 for a variable corresponds to the lower bound of the design space, while a value of 1 corresponds to the upper bound. Figure 17 shows instead a visual representation of the optimized design variables.

It can be observed that the kink point y_{kink} has been moved toward the wing root, the tip twist θ_{tip} has increased, and the horizontal tail scale has also increased compared to the HERA UCB baseline configuration considered for this study, by 30.0%, 41.3%, and 25.2%, respectively. The position of the propellers y_{eprop} has shifted toward the wingtip, moving from 20.0% in the baseline to 45.2%.

From an aerodynamic perspective, shifting the propellers outward is beneficial for the wing L/D ratio. However, this shift also increases the wing bending moment due to the engines weight. While this moment can initially counterbalance the opposite moment generated by lift, if it becomes too large, it requires higher wing structural mass to withstand it.

Regarding structural variables, the spar cap area has been reduced by 7%, while the stringer area reaches the lower limit of the design space. The correlation between the optimization results with and without surrogate models can be evaluated by comparing the second and third columns of each group. The variables showing the greatest deviations are the wing tip twist and the propeller position, each differing by about 8% within the design space. This deviation is likely due to the lower, but still relevant, sensitivity of these variables to the overall aircraft range, compared to the others. Figure 18 (b) instead shows the results for the objectives, specifically the aircraft's L/D ratio, the wing mass, and the aircraft range (the actual objective is solely the range, but both the L/D ratio and the wing

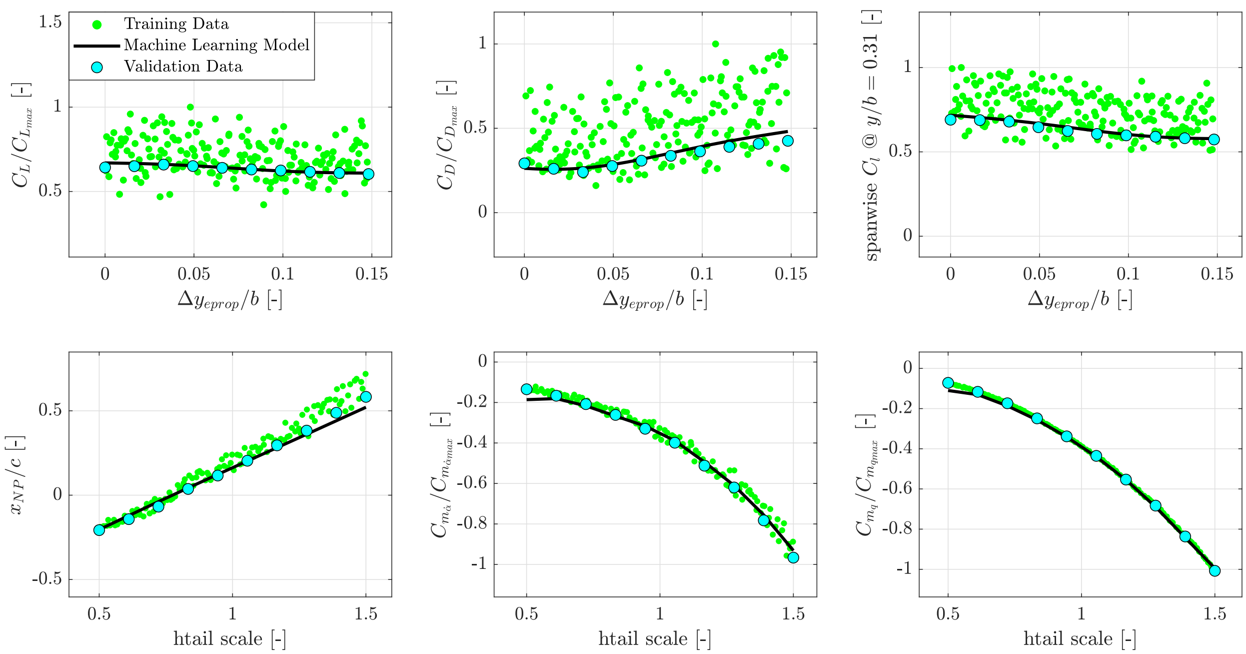

Figure 16. Slices of Surrogate models for the aerodynamic and stability discipline outputs. Training data (dependent on multiple variables), Surrogate data (slice), Validation points (slices).

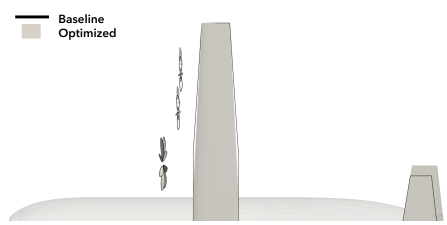

Figure 17. Optimization result geometry.

mass contribute to it and are therefore represented as interesting subjects of analysis). It can be observed that the optimization result leads to an increase in aircraft L/D of 9.00% and a reduction in wing mass of 16.25% compared to the HERA baseline configuration. This results in an increase in range of 19.06%, in accordance with the Breguet range equation 6. The correlation between the objective results with and without surrogate models is again acceptable: for the L/D ratio, wing mass, and range, deviations are 0.80%, 0.55%, and 0.50%, respectively despite the discrepancies in the design variables observed in Figure 18 (a).

Figure 19 (a) shows the optimization path of the objective function, the range, over the first 150 iterations of the optimization process. The comparison between the optimization performed with and without the use of surrogate models highlights a similarity not only in the final result but also in the actual optimization trajectory. This consistency confirms the reliability of the DOE-based approach using surrogate models for the aerodynamic disciplines.

Figure 19 (b) also shows the Pareto front obtained from an iterative cycle of optimizations, using as objective of minimization the wing mass, and putting an incremental constraint on the aircraft's L/D. The Pareto front is depicted in figure 19 (b) with respect to the wing mass and aircraft L/D, nondimensionalized with respect to the baseline HERA values. The Pareto front represents the set of optimal trade-off solutions in a multi-objective problem, and solutions lying on this front are called Pareto optimal points, while those that are outperformed in all objectives by other solutions are referred to as Pareto dominated points. It can be observed that the original optimization, using as objective the range of the aircraft, selects a specific point on the Pareto optimal (PO) front, thus providing an optimal balance between the minimization of the wing mass and the maximization of the aircraft L/D ratio. From figure 19(b), it is also possible to observe the comparison between the optimization results with and without surrogate models, which match the values already shown in figure 18 (b). An additional point is also displayed, showing the mass and L/D ratio corresponding to the geometry optimized using surrogate-based disciplines, but evaluated using DUST (verification point). The results from the surrogate model and the verification point differ from the non-surrogate optimization result in terms of R_e with deviations of 0.55% and 0.179% for mass, and 0.80% and 0.183% for L/D.

Table 8 shows the computational times associated with the optimization process with and without surrogate models, including the training times of the surrogate disciplines. There are four surrogate disciplines in total: the first one related to aerodynamic loads, and the other three related to aerodynamic stability. The reason for splitting the latter into three separate models is that each derivative requires dedicated simulations, following the methodology described in (Ref. 27).

It can be observed that, in this specific case, the total optimization time, including training, is approximately 49% of the time required when surrogate models are not used. Nevertheless, these models achieve acceptable accuracy, as shown in Figure 16 and Table 7. The computational time advantage are greater than those observed in the trim problem discussed in the previous section, due to the larger number of iterations required for the optimizer to converge.

Table 8. Optimization computational time.

$t_{wo/surr}$	t_{train}		$t_{w/surr}$	$tot_{surrogate}$	$\%adv$
66h 15m	Aero loads	6h 40m	4m 55s	32h 28m	-49.01%
	Static $C_{j\alpha}$	13h 19m			
	Plunge $C_{j_{\dot{\alpha}}}$	6h 12m			
	Phugoid C_{jq}	6h 12m			

Figure 20 (a) shows the evolution of the constraint on the static stability margin of the aircraft, expressed as the difference in percentage between the neutral point of the aircraft and the center of gravity, which are both varying within the optimization history. It is shown that the implemented framework can effectively consider this constraint while optimizing the configuration. The optimization path for the $S.M.$ is predominantly driven by the horizontal tail scale design variable, which plays a major role in determining the static stability characteristics of the aircraft (see Figure 16), while the influence of the variation of the mass and aerodynamic properties of the wing but has a secondary effect. The $S.M.$ enters the feasibility region relatively early in the optimisation loop, showing that it is effectively controlled by the parametrization on the tail plane scale.

Figure 20 (b) shows the evolution of the constraints on the frequency and damping of the short period mode throughout the optimization process. According to Cook (Ref. 23), the $\omega_s - \zeta_s$ diagram includes a region (the so-called fingerprint graph) identified as satisfactory by pilot opinion in terms of flying qualities. Within this region, the aircraft exhibits acceptable maneuverability (initial response) without being overly sensitive to control inputs, and with well-damped oscillations. It can be observed that the effect of the constraint during the optimization is to drive the aerodynamic and mass properties of the aircraft into the satisfactory FQ region. The horizontal tail scale emerges as the dominant driver of the short period characteristics (see m_{Y_α} in Eq.4), while the main wing's mass and aerodynamic changes provide secondary contributions.

CONCLUSIONS

A multi-disciplinary analysis, trim, and optimization were carried out on the Clean Aviation HERA UCB configuration. This work focused on the extension of an aero-structural optimization framework with trim capabilities to the modelling of flying qualities constraints for the aircraft developed within the Clean Aviation HERA project. The MDO framework built around GEMSEO enabled modular integration of DUST models. The framework supported the generation of surrogate models trained using machine learning regression in the multi-disciplinary loop. A multi-fidelity optimisation is performed in that full-order and surrogate based optimisation is compared.

In particular, a complete DUST model of HERA was created and implemented in the MDO framework. The model was verified against a RANS solution obtained with the TAU solver. The aerodynamic analysis showed that interactional aerodynamic effects can be exploited to optimize the DEP (Distributed Electric Propulsion) configuration. Subsequently, using the developed framework, trim analysis and aero-structural optimization of the configuration were performed. The optimization led to a configuration optimized in terms of aircraft range, by minimizing wing mass and maximizing aerodynamic efficiency. The results showed very good correlation between the surrogate model predictions and the time-marching simulation results. The methodology for implementing stability and flying qualities constraints was therefore verified, demonstrating its crucial value during design to ensure that the aircraft achieves the desired flight performance.

ACKNOWLEDGEMENTS

This project has received funding from the Clean Aviation Joint Undertaking under the European Union's Horizon Europe research and innovation programme under Grant Agreement HERA (Hybrid-Electric Regional Architecture) n° 101102007. Views and opinions expressed are however those of the author(s) only and do not necessarily reflect those of the European Union or CAJU. Neither the European Union nor the granting authority can be held responsible. The authors thank Jose Fernandez Montes for his valuable support in the integration of the structural sizing discipline and Sven Lanzan Ferran for the feedback on the multidisciplinary design framework. Thanks to Daniela Gisele Francois from DLR for the support on the TAU setup.

HERA CLEAN AVIATION Co-funded by the European Union

Daniele Granata would like to thank the support by PNRR 118 – TDA, Cycle 39 – Transitions (Ministerial Decree 118/23), funded by the European Union – Next Generation EU, Mission 4 Component 1. CUP: D43C23002740001

Finanziato dall'Unione europea NextGenerationEU · Ministero dell'Università e della Ricerca · Italiadomani PIANO NAZIONALE DI RIPRESA E RESILIENZA · POLITECNICO MILANO 1863

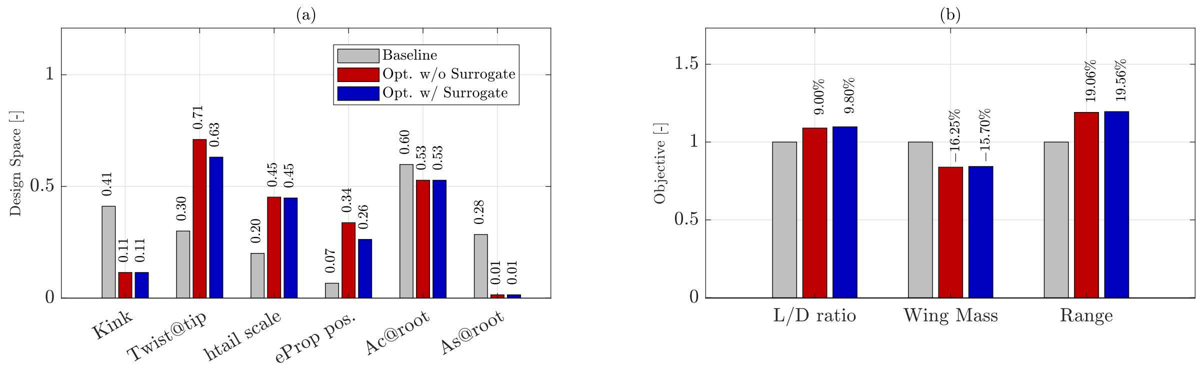

Figure 18. MDO final results, design variables and Objectives. Comparison between Baseline configuration, optimized with surrogate, and optimized without the surrogate.

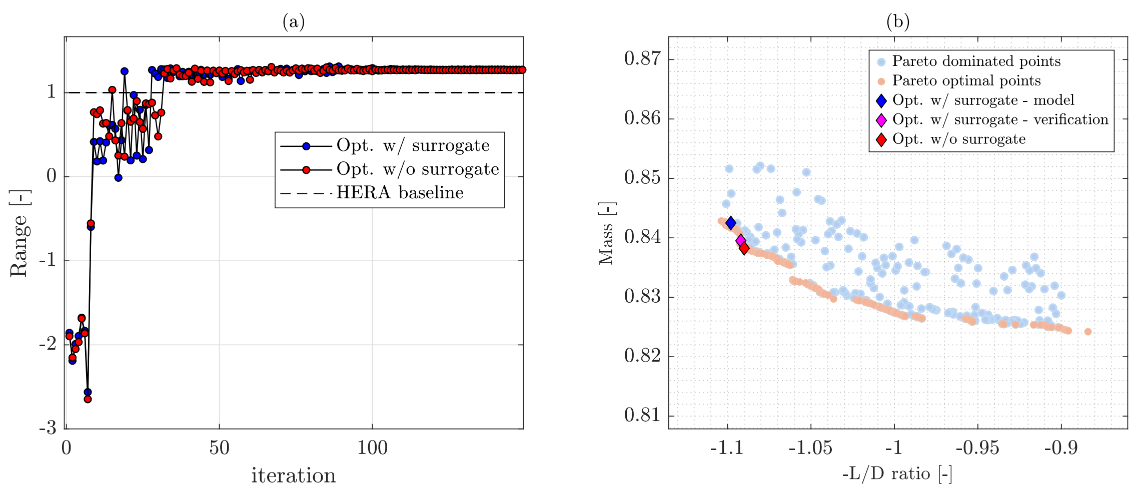

Figure 19. (a) Objective Function convergence (b) Mass-L/D ratio Pareto Optimal front, and optimzed configuration predicted with and without surrogate model for aerodynamic loads.

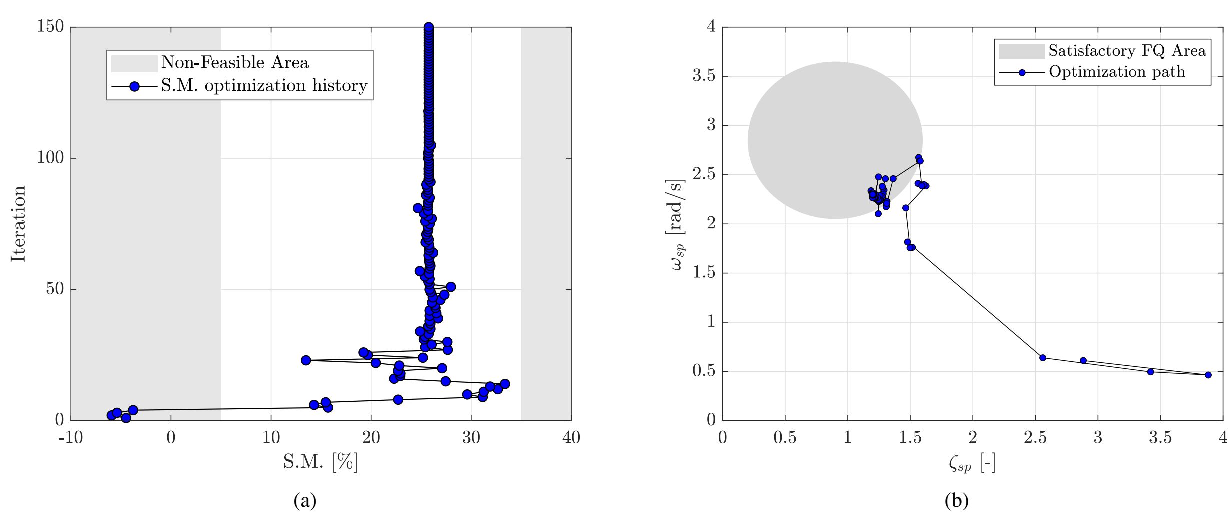

Figure 20. (a) Static margin constraint optimization history. (b) Short Period constraint on the finger-print short-period flying qualities graph.

REFERENCES

1. Joon W Lim. Fundamental investigation of proprotor and wing interactions in tiltrotor aircraft. In *Proceedings of the 75th Annual Vertical Flight Society Forum and Technology Display, Philadelphia, PA, USA*, pages 13–16, 2019.

2. Alberto Savino, Alessandro Cocco, Alex Zanotti, Vincenzo Muscarello, et al. Numerical investigation of wing-propeller aerodynamic interaction through a vortex particle-based aerodynamic solver. In *48th European Rotorcraft Forum (ERF 2022)*, pages 1–9. Curran, 2022.

3. Alex Zanotti, Luca Menini, Alberto Savino, Donato Grassi, and Luca Riccobene. Experimental investigation of wing-propeller aerodynamic interaction in evtol configurations. *Aerospace Science and Technology*, 152:109348, 2024.

4. C. Niro, A. Savino, A. Cocco, and A. Zanotti. Mid-fidelity numerical approach for the investigation of wing-propeller aerodynamic interaction. *Aerospace Science and Technology*, 108950, 2024.

5. Geng Qiao and George N Barakos. Aerodynamic study of wingtip-mounted propeller and distributed propulsion system. In *Proceedings of the 49th European Rotorcraft Forum (ERF)*, Rotterdam, The Netherlands, 2024.

6. Eric S Hendricks, Eliot Aretskin-Hariton, Daniel Ingraham, Justin S Gray, Sydney L Schnulo, Jeff Chin, Robert Falck, and Dustin Hall. Multidisciplinary optimization of an electric quadrotor urban air mobility aircraft. In *AIAA Aviation 2020 Forum*, page 3176, 2020.

7. Ö Petersson and F Daoud. *Multidisciplinary optimization of aircraft structures with respect to static and dynamic aeroelastic requirements*. Deutsche Gesellschaft für Luft-und Raumfahrt-Lilienthal-Oberth eV, 2012.

8. Anne Gazaix, François Gallard, Vincent Ambert, Damien Guénot, Maxime Hamadi, Stéphane Grihon, Patrick Sarouille, Thierry Y Druot, Joël Brézillon, Vincent Gachelin, et al. Industrial application of an advanced bi-level mdo formulation to aircraft engine pylon optimization. In *AIAA Aviation 2019 Forum*, page 3109, 2019.

9. Neal T Frink, Brett R Hiller, Patrick C Murphy, Kevin Cunningham, and Gautam H Shah. Investigation of reduced-order modeling for aircraft stability and control prediction. In *AIAA Scitech 2019 Forum*, page 0980, 2019.

10. Daniele Granata, Alberto Savino, and Alex Zanotti. Numerical evaluation of aircraft aerodynamic static and dynamic stability derivatives by a mid-fidelity approach. *Aerospace*, 11(3):213, 2024.

11. Politecnico di Milano. DUST, https://www.dust.polimi.it/.

12. GEMSEO Documentation. GEMSEO: Generic Engine for Multi-disciplinary Scenarios, Exploration, and Optimization https://gemseo.readthedocs.io/en/stable/index.html.

13. Matteo Tugnoli, Davide Montagnani, Monica Syal, Giovanni Droandi, and Alex Zanotti. Mid-fidelity approach to aerodynamic simulations of unconventional vtol aircraft configurations. *Aerospace Science and Technology*, 115:106804, 2021.

14. DLR. TAU, https://www.dlr.de/en/as/research-and-transfer/software-solutions/aerodynamics/software-tau.

15. Alberto Savino, Alessandro Cocco, Alex Zanotti, Matteo Tugnoli, Pierangelo Masarati, and Vincenzo Muscarello. Coupling mid-fidelity aerodynamics and multibody dynamics for the aeroelastic analysis of rotary-wing vehicles. *Energies*, 14(21):6979, 2021.

16. Blake B Hillier, Mark J Stock, and Adrin Gharakhani. Robust and corrected coefficients for the rotor-body-interaction body. *AIAA Journal*, 59(10):4281–4283, 2021.

17. Peter D. Gray. Neuralfoil - a neural network-based airfoil performance predictor. https://github.com/peterdsharpe/AeroSandbox, 2023.

18. A Mateo-Gabín, T. Wagenaar, Mancini S., et al. Analysis and optimization of a distributed propulsion system for a regional transport aircraft. In *9th European Congress on Cimputational Methods in Applied Sciencies and Engineering (ECCOMAS 2024)*, pages 1–13, 2024.

19. Andrés Mateo, Marta A. Martín, Jose Fernandez, Sven A. Lanzan Ferran, Simone Mancini, and Tim Klaproth. *An AI-Enhanced Multidisciplinary Optimization Framework for Net-Zero Transport Aircraft*.

20. DLR. CPACS: https://dlr-sl.github.io/cpacs-website.

21. J. Fernández Montes. *Optimización de Parámetros de Ala Mediante Algoritmos Genéticos*. Universidad Politécnica de Madrid, Madrid, 2015.

22. Andrés Mateo-Gabín, Simone Mancini, Marta A. Martín, Jose Fernández Montes, Sven A. Lanzan Ferran, and Tim Klaproth. An ai-enhanced multidisciplinary optimization framework for net-zero transport aircraft. In *AIAA 2025, Las Vegas*, pages 1–18, 2025.

23. Michael V Cook. *Flight dynamics principles: a linear systems approach to aircraft stability and control*. Butterworth-Heinemann, 2012.

24. Douglas C Montgomery. *Design and analysis of experiments*. John wiley & sons, 2017.

25. B Omede, AM Grande, et al. Machine learning and numerical optimization of bio-inspired 3d-printable sandwich core cell. In *ICAS PROCEEDINGS*, pages 1–17. International Council of the Aeronautical Sciences, 2024.

26. Jianguang Fang, Guangyong Sun, Na Qiu, Nam H Kim, and Qing Li. On design optimization for structural crashworthiness and its state of the art. *Structural and Multidisciplinary Optimization*, 55:1091–1119, 2017.

27. Daniele Granata, Alberto Savino, and Alex Zanotti. Evaluation of a mid-fidelity approach for the calculation of tiltrotor aerodynamic stability derivatives in cruise flight conditions. *Aerospace Science and Technology*, page 110384, 2025.